Received: 30 September 2019 | Revised: 22 November 2019 | Accepted: 2 December 2019

DOI: 10.1002/mrc.4978

WILEY

RESEARCH ARTICLE

Spectral deconvolution in electrophoretic NMR to investigate the migration of neutral molecules in electrolytes

Florian Schmidt[1] | **Andrea Pugliese**[2] | **Catherine C. Santini**[3] | **Franca Castiglione**[2] | **Monika Schönhoff**[1]

[1]Institute of Physical Chemistry, University of Muenster, Münster, Germany

[2]Department of Chemistry, Materials and Chemical Engineering Giulio Natta, Politecnico di Milano, Milan, Italy

[3]Institut de Chimie de Lyon, UMR 5265 CNRS-C2P2, Université de Lyon, Lyon, France

Correspondence
Monika Schönhoff, Institute of Physical Chemistry, University of Muenster, Corrensstr. 28/30, 48149 Münster, Germany.
Email: schoenho@uni-muenster.de

Abstract

Electrophoretic nuclear magnetic resonance (eNMR) is a powerful tool in studies of nonaqueous electrolytes, such as ionic liquids. It delivers electrophoretic mobilities of the ionic constituents and thus sheds light on ion correlations. In applications of liquid electrolytes, uncharged additives are often employed, detectable via ^{1}H NMR. Characterizing their mobility and coordination to charged entities is desirable; however, it is often hampered by small intensities and ^{1}H signals overlapping with major constituents of the electrolyte. In this work, we evaluate methods of phase analysis of overlapping resonances to yield electrophoretic mobilities even for minor constituents. We use phase-sensitive spectral deconvolution via a set of Lorentz distributions for the investigation of the migration behavior of additives in two different ionic liquid-based lithium salt electrolytes. For vinylene carbonate as an additive, no field-induced drift is observed; thus, its coordination to the Li^{+} ion does not induce a correlated drift with Li^{+}. On the other hand, in a solvate ionic liquid with tetraglyme (G4) as an additive, a correlated migration of tetraglyme with lithium as a complex solvate cation is directly proven by eNMR. The phase evaluation procedure of superimposed resonances thus broadens the applicability of eNMR to application-relevant complex electrolyte mixtures containing neutral additives with superimposed resonances.

KEYWORDS

^{1}H, ^{7}Li, ^{19}F, battery electrolytes, electrophoretic NMR, ionic liquid, lithium transport, NMR, phase analysis, PFG-NMR

1 | INTRODUCTION

The electrolyte plays a crucial role for the performance of a battery. The very demanding requirements concerning battery electrolytes led to a variety of approaches towards new types of electrolytes.[1,2] With the aim to resolve safety issues, less volatile/flammable liquid electrolytes based on ionic liquids (ILs) were considered. However, these electrolytes consisting of a Li salt in an IL usually suffer from high viscosities and low conductivities. In

order to improve their properties, neutral additives are employed with the intention of either improving the electrode–electrolyte interface (solid electrolyte interface), or advancing the lithium transport by weakly coordinating molecules, which compete with the Li–anion interaction. A variety of studies on the impact of additives on the lithium dynamics in IL electrolytes has been carried out using nuclear magnetic resonance (NMR), electrochemical methods, and molecular dynamics simulation techniques.[3–9] Impedance measurements deliver the total conductivity, but do not distinguish between the contributions from different charge carriers. Diffusion NMR measurements, on the other hand, deliver ion-specific information. Assuming validity of the Nernst–Einstein equation, transference numbers and thus the contributions of particular ion species to the conductivity can be determined.[10–12] In concentrated electrolytes, however, ion correlations such as ion pair formation may play a large role, as shown for a range of different systems.[13–17] In that case, the information content of diffusion coefficients is limited, and an interpretation in terms of single ions, pairs, or clusters requires complex models.[18]

Recently, electrophoretic NMR (eNMR) was introduced to the field of IL-based electrolytes.[13,19] The method provides the ability to directly investigate the migration velocities of charged and neutral molecules in an electric field and benefits from the species selectivity that comes with NMR spectroscopy.[20,21] Typically, the investigated nuclei in battery electrolytes are ^{7}Li, ^{1}H contained in the solvent and/or the IL cation, and ^{19}F contained in the investigated anion. The eNMR experiment consists of a pulsed field gradient NMR diffusion experiment with additional simultaneous electric field pulses applied to the investigated sample. The application of the electric field causes a coherent displacement of the investigated nuclei, resulting in a phase shift ϕ-ϕ_0 of the observed NMR signal phase, as compared with the signal without electric field, ϕ_0.[20,22]

With this technique, Li transference numbers in IL were determined without assumption of an ideal electrolyte, that is, in a model-free approach without assuming validity of the Nernst–Einstein equation. A large influence of Li–anion correlations was found, which even results in an unintended lithium migration in the "wrong" direction caused by strong lithium–anion correlations leading to the transport of net negatively charged clusters.[23–26] This was termed a "vehicle mechanism" of Li transport, and after being experimentally observed in several salts,[23,26] it was confirmed by simulations and suggested as a generic feature in Li salt in IL systems.[25]

As drift velocities become experimentally accessible, the role of uncharged additives in IL-based electrolytes is interesting to clarify. However, due to typically low concentrations, low mobilities, and overlapping ^{1}H signals from different compounds, this has not been achieved so far.

In dilute aqueous salt solutions, however, where experimentally observable phase shifts can reach >1,000°,[22] eNMR is established in the investigation of multiple molecular species, which exhibit different phase shifts in the ^{1}H eNMR spectrum.[22,27–29] It was shown that the mobilities can be analyzed via 2D Fourier transformation applying the States–Haberkorn correction yielding a mobility-ordered spectrum (MOSY).[22,30] This has been demonstrated as a powerful tool to resolve superimposed ^{1}H eNMR spectra of, for example, aqueous amino acid mixtures or polyelectrolytes and their counterions by their electrophoretic mobilities.[28,31–35]

Unfortunately, when investigating ILs, which have a high viscosity, the observable phase range is significantly less than in aqueous systems due to lower mobilities and higher conductivities, which limit the applicable electric fields.[13,19] Additionally, the electrodes in the NMR sample tube significantly disturb the homogeneity of the static magnetic field and decrease the spectral resolution. Thus, the applicability of MOSY spectra to distinguish distinct molecular species in ILs with small mobility differences is limited.

In the present work, we introduce the phase-sensitive spectral deconvolution of eNMR spectra in order to investigate the correlated migration behavior of additives in IL–lithium salt mixtures and to overcome spectral and phase resolution issues. ^{1}H eNMR measurements are performed on two different IL-based lithium salt electrolytes with either added vinylene carbonate (VC) or tetraglyme (G4). The first mixture consists of 1 mol L^{-1} LiTFSA in C_1C_6ImTFSA + 5 % (per volume) VC, that is, $Li(C_1C_6Im)_3(TFSA)_4(VC)_{0.8}$, which was investigated in the past by NMR spectroscopy, diffusion experiments, and molecular dynamics simulations.[8] The second mixture consists of the solvate IL $Li(G4)_1TFSA$[36,37] and the IL C_1C_2ImTFSA at a molar ratio of 1:8 resulting in the sum formula $Li(G4)_1(C_1C_2Im)_8(TFSA)_9$. Considering previous work on solvate IL, one expects the formation of a complex solvate cation effectively breaking unwanted lithium–anion clusters. The ^{1}H eNMR spectra of these mixtures exhibit superimposed ^{1}H NMR signals of the respective imidazolium-based cation and the additive. We compare the results of the proposed deconvolution method with MOSY 2D fast Fourier transformation processed spectra and phase data obtained from zero-order phase correction. Finally, we achieve the determination of the mobilities of additives, even if they are present in minor amounts and even if ^{1}H resonances are overlapping. With the aforementioned two electrolytes,

we can showcase a system with and without pronounced additive drift, respectively. This first determination of additive mobilities opens the route for studies of the transport of additive species in further electrolyte formulations.

2 | EXPERIMENTAL

2.1 | Materials

5 vol% of VC (Aldrich > 99%) was added to a mixture of 1 mol L^{-1} lithium bis-(trifluoromethanesulfonyl)amide (LiTFSA, Sigma Aldrich ≥ 99%) in 1-hexyl-3-methylimidazolium bis-(trifluoromethanesulfonyl) amide (C_1C_6ImTFSA). C_1C_6ImTFSA was synthesized by Bolimowska et al. as reported previously.[8] LiTFSA, tetraethylene glycol dimethyl ether (tetraglyme, G4, Sigma Aldrich ≥ 99%), and 1-ethyl-3-methyl-imidazolium bis-(trifluoromethanesulfonyl)amide (C_1C_2ImTFSA, Iolitech ≥99%) were mixed with a molar composition of $Li(G4)_1(C_1C_2Im)_8TFSA_9$.

2.2 | eNMR experiments

Experimental data were acquired on a 400 MHz Avance III HD NMR spectrometer (Bruker), equipped with a Diff50 probe head, and a 400 MHz Avance spectrometer (Bruker), equipped with a Diff30 probe head. A double stimulated echo pulse sequence with gradient pulses[38] was used while applying alternating electric field pulses with an in-house built power source. The electric fields were incremented from low to higher voltages while keeping all parameters of the pulse program constant. The observation times (Δ) were between 100 and 200 ms, and the gradient pulse duration (δ) was between 0.5 and 3 ms, depending on the investigated nucleus. A customized sample cell, based on the cylindrical design of Holz,[20] was equipped with capillaries and palladium electrodes spaced at a distance of 22 mm as described earlier.[13] The capillaries and the sample cell were dried at high vacuum and 105°C overnight prior to filling the tube with electrolyte solutions in an argon-filled glove box. The ^{1}H chemical shift was referenced to 8 ppm for the ^{1}H signal of the C^2 carbon atom of the imidazolium ring in $C_1C_2Im^+$, as determined for an imidazolium-based IL with the TFSA counter ion.[39]

2.3 | Data evaluation

The python modules nmrglue,[40] lmfit, matplotlib, numpy,and pandas were used for the import, processing, and fitting of all results. For the MOSY processing, zero filling up to 32 k data points in the indirect dimension was applied, and the peak height was determined by selecting the largest value.

3 | PHASE ANALYSIS METHODS

eNMR measurements yield spectra with a phase shift depending on the drift velocity of the respective ion species. This phase shift is directly proportional to the gyromagnetic ratio γ, the magnetic field gradient pulse duration δ and strength g, the observation time Δ, and the drift velocity ν (see Equation (1)). The drift velocity is directly proportional to the applied electric field E and the electrophoretic mobility μ of the respective molecular species (see Equation (2)).

$$\phi - \phi_0 = \gamma \delta \Delta g \nu \tag{1}$$

$$\nu = \mu E \tag{2}$$

The phase shift $\phi - \phi_0$ needs to be quantified in order to derive the observed nuclei's mobility. Generally, the phase angle ϕ of a spectrum is defined by Equation (3), where S_0 is the amplitude, $A(\omega)$ the absorptive, and $D(\omega)$ the dispersive spectrum.

$$S(\omega) = S_0[A(\omega) + iD(\omega)]\exp(i\phi) \tag{3}$$

The simplest approach towards determining ϕ is to multiply the acquired spectrum with exp (iϕ_{corr}) varying ϕ_{corr} until ϕ = -ϕ_{corr}, such that the exponential term in Equation (3) becomes zero, obtaining a purely absorptive spectrum.[41] This process of "phasing" the spectrum is often done manually under visual inspection of the resulting spectrum. For the series of spectra with individual phases acquired in eNMR, this procedure is time consuming and limited in its accuracy due to a personal bias. In addition, this approach is limited to spectra consisting of single resonances without any superposition by other resonances with a different phase shift. Regarding phase correction, one distinguishes between zero and first-order phase correction, in order to correct frequency-independent and frequency-dependent phase distortions. In the context of eNMR, only zero-order phase correction is typically applied to extract ϕ_{corr} from the phase value required to obtain a purely absorptive spectrum.

In order to overcome the drawbacks of manual phase determination, we describe the following three different approaches towards analyzing the signal phase shift. Further on, we compare them with regard to their performance in eNMR measurements investigating nuclei with low mobilities.

3.1 | Entropy minimization

A variety of phase correction algorithms was introduced in the past in order to automatize and improve the phasing process of NMR spectra.[42–45] A robust algorithm was described as a method for phase correction of NMR spectra by Chen et al.[46] It involves an entropy minimization, based on the fact that purely absorptive spectra exhibit lower entropies than purely dispersive spectra. With the first derivative of the spectrum h_j, the entropy S is calculated via Equation (4) and minimized by performing zero-order phase correction.

$$S = -\sum\nolimits_i h_j ln h_j \tag{4}$$

The application of zero-order phase correction as a tool for the analysis of signal phase shifts requires that the investigated NMR spectrum consists only of a single component exhibiting a single mobility. In particular, it is not possible to distinguish between different phase shifts of superimposed signals. Therefore, this method is not further considered for the analysis of superimposed eNMR resonances, but can be used on isolated resonances.

3.2 | 2D fast Fourier transformation (MOSY)

Applying the Euler formula to Equation (3) and inserting Equations (1) and (2) result in Equation (5). It becomes clear that the phase shift of the observed NMR signal can be described as an oscillation of the signal intensity in dependency of the applied electric field E, electrophoretic mobility μ, observation time Δ, gradient strength g, and the gradient duration δ.

$$S(\omega) = S_0[A(\omega) + iD(\omega)][\cos(\gamma\delta\Delta g\mu E) + i\sin(\gamma\delta\Delta g\mu E)] \tag{5}$$

Therefore, the electrophoretic mobility can be analyzed via 2D Fourier transformation in the time domain and the electric field domain E, using a modification of the States–Haberkorn method as applied in various reports.[22,27–29] The States method is employed to obtain pure absorption phase spectra and suppress phase twist line shapes.[30] For its application, the voltage must be incremented linearly, covering both positive and negative voltage regions. The data for each frequency ω are then transformed individually, yielding a 2D correlation plot of electrophoretic mobility versus frequency.

3.3 | Fitting of Lorentz profiles

Alternatively, for the analysis of phase modulations in eNMR measurements, a phase-sensitive spectral deconvolution of eNMR spectra can be performed. The benefit of this approach is to extract more precise phase information by correlating data from all frequencies ω, which belong to the same signal, and therefore must exhibit the same phase shift. A limitation of this approach is that an assumption of a particular line shape is necessary; here, we employ a set of Lorentzian profiles.

The absorptive $A(\omega, \omega_L, \lambda)$ and dispersive Lorentz profile $D(\omega, \omega_L, \lambda)$, depending on the nuclei's resonance frequency ω_L, and the coherence decay rate constant λ, which is proportional to the peak width λ/π, are given in Equation (6).

$$\begin{aligned} A(\omega,\omega_L,\lambda) &= \frac{\lambda}{\lambda^2 + (\omega-\omega_L)^2} \\ D(\omega,\omega_L,\lambda) &= \frac{-\omega-\omega_L}{\lambda^2 + (\omega-\omega_L)^2} \end{aligned} \tag{6}$$

The real R_i and imaginary I_i parts of a NMR spectrum are then given as a trigonometric combination of absorptive and dispersive Lorentzians according to Equations (7a) and (7b) with a as the amplitude and ϕ as the signal phase. In the case of $\phi = 0$, one obtains a purely absorptive spectrum for R_i and a purely dispersive spectrum for I_i.[41]

$$R_i = |a|(A(\omega,\omega_L,\lambda)\cos\phi - D(\omega,\omega_L,\lambda)\sin\phi) \tag{7a}$$

$$I_i = |a|(D(\omega,\omega_L,\lambda)\cos\phi + A(\omega,\omega_L,\lambda)\sin\phi) \tag{7b}$$

$$\hat{S}(\omega,\omega_i,\lambda_i,a_i,\phi_i,b) = b + \sum\nolimits_{i=1}^{n_p}[R_i[\omega,\omega_i,\lambda_i,a_i,\phi_i] + iI_i[\omega,\omega_i,\lambda_i,a_i,\phi_i]] \tag{8}$$

For the analysis of an eNMR data set, each recorded spectral row corresponding to an applied voltage is approximated individually via the sum of a set of Lorentzians. The complex phase-sensitive spectral shape

is given by Equation (8), where n_p is the number of peaks to be fitted, b the baseline, and ω_i, λ_i, a_i and ϕ_i are individual parameters for each fitted peak according to Equation (6).

In order to reduce the degrees of freedom of the fit model, reasonable restrictions to the fit function may be introduced, for example, using the same phase ϕ_i for peaks that are assigned to the same molecule and therefore will exhibit the same signal phase shift.

This approach correlates all frequencies with each other and considers physically meaningful dependencies of correlated resonances, while being able to describe superimposed signals. Additionally, the individual phase values for each electric field value E are obtained, which makes it easier to test their linearity and thus identify potential experimental artifacts.

4 | RESULTS AND DISCUSSION

4.1 | VC in LiTFSA/C_1C_6ImTFSA

The mixture of VC with 1 mol L^{-1} LiTFSA in C_1C_6ImTFSA was investigated via ^{1}H, ^{7}Li, and ^{19}F eNMR. In the ^{1}H spectrum, the low VC concentration results in only a minor VC signal, which is furthermore overlapping with the ^{1}H resonances of $C_1C_6Im^+$ (see Figure S1). Two regions of the full ^{1}H eNMR spectrum were selected for the analysis of the $C_1C_6Im^+$ and VC mobilities. The first region exhibits the C^4 and C^5 ^{1}H signals (7.1–6.6 ppm) of the organic cation's imidazolium ring as well as the ^{1}H signal of VC (see Figure 1), whereas the second region (2 to −0.5 ppm) exhibits solely isolated alkyl ^{1}H signals of $C_1C_6Im^+$ and serves as reference for the Lorentz fitting method. The ^{1}H spectra of the VC region acquired with −200, 0, and + 200 V are depicted in Figure 1 (see black lines) exhibiting only minor phase variations, which could be mistaken for random phase errors. However, it is not apparent from this depiction whether all three peaks exhibit the same or deviating phase shifts, respectively.

4.1.1 | Mobility-ordered spectroscopy

The ^{1}H MOSY spectrum was calculated for the first spectral region (7.1–6.6 ppm) containing the VC signal of the investigated VC/LiTFSA/C_1C_6ImTFSA mixture and is shown in Figure 2a. The two peaks labeled as $C^{4/5}$ correspond to the adjacent aromatic protons in $C_1C_6Im^+$, whereas VC corresponds to the proton signal in VC. Due to the nature of Fourier transformation, the resolution of the resulting MOSY spectrum is strongly dependent on the number of oscillation periods recorded in the indirect dimension. Unfortunately, the observable phase shift range in eNMR measurements of viscous, highly concentrated solutions is often limited to $<\pi/2$. In the presented example, only a very minor distinction between the $C^{4/5}$ and VC signals can be made in the mobility dimension of Figure 2a.

Slices of the MOSY spectrum corresponding to the chemical shifts of the discussed signals are extracted (see Figure 2b), in order to obtain a better comparison of the peaks of interest and the mobility differences. Electrophoretic mobilities obtained from the respective maxima are indicated in Figure 2b. Both $C^{4/5}$ signals (δ: 6.91 and 6.84 ppm), exhibit approximately the same mobility but deviate from each other by approximately $0.3{\cdot}10^{-10}$ m^2 V^{-1} s^{-1}. VC exhibits a peak maximum at $1.4{\cdot}10^{-10}$ m^2 V^{-1} s^{-1}. However, this maximum is very broad, indicating a considerable error. In addition, considering the low intensity, the overlapping $C^{4/5}$ signals may influence the position of the maximum. Thus, although both $C^{4/5}$ signals are clearly occurring at positive mobilities, it is hard to state whether the small positive value of VC is an overlap-induced artifact, or indicates a true drift of VC. Thus, in this application involving viscous samples where only small phase changes are observed, the analysis of MOSY-processed eNMR is limited.

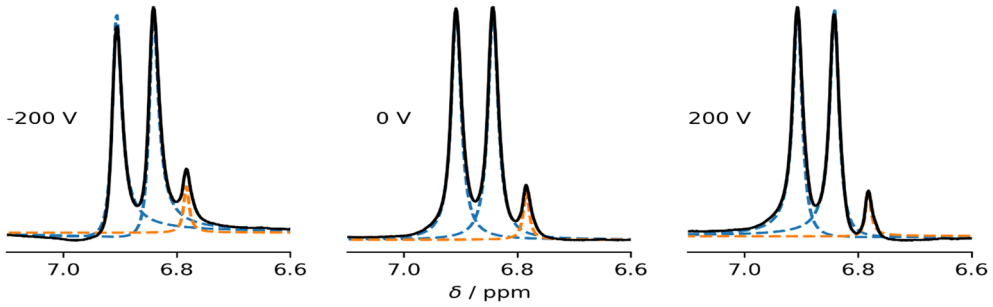

FIGURE 1 Black lines: ^{1}H electrophoretic nuclear magnetic resonance spectra of VC/C_1C_6ImTFSA/LiTFSA at −200, 0, and 200 V in the spectral region containing the $C^{4/5}$ ^{1}H signals of the imidazolium ring and the smaller vinylene carbonate signal. Dashed lines: Lorentzian fits ($C^{4/5}$: blue dashed lines, vinylene carbonate: orange dashed line)

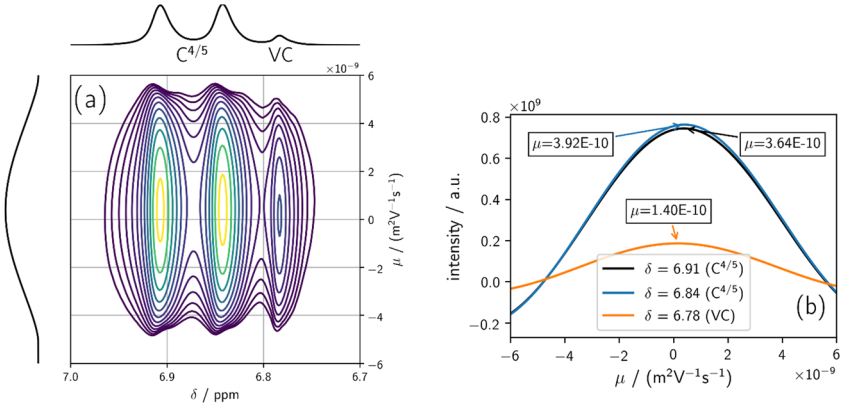

FIGURE 2 (a) ^{1}H mobility-ordered spectrum of spectral vinylene carbonate and $C^{4/5}$ region and (b) slices of the ^{1}H mobility-ordered spectrum for the $C^{4/5}$ ($\delta = 6.91$ ppm and $\delta = 6.84$ ppm) and VC ($\delta = 6.78$ ppm) peaks

4.2 | Lorentz fitting procedure

Both spectral regions were fitted individually with a superposition of three Lorentzians. For the first spectral region (7.1–6.6 ppm), examples of the fit are shown in Figure 1 by dashed lines. Here, the phase, amplitude, and peak width of the two $C_1C_6Im^+$ signals were set to identical values, respectively. For a separate fit of the second spectral region (2 to −0.5 ppm), the phase was set equal for all isolated ^{1}H alkyl signals. These physically meaningful restrictions to the fit models were introduced in order to reduce the degrees of freedom by correlating not only frequencies of a single signal but also of multiple signals, which belong to the same molecular species.

The phase shift values obtained for the superimposed VC and $C_1C_6Im^+$ signals of the first spectral region are depicted in Figure 3a and clearly deviate from each other. The second spectral region was analyzed as well by spectral deconvolution, resulting in the phase data in Figure 3b (see full blue circles). For comparison, we also performed an analysis via phase correction, these data (open circles in Figure 3b) are in very good agreement with the fit results, showing that the phase correction method and the fitting method yield equivalent results, if no superposition is present. In addition, the phase shift values of $C_1C_6Im^+$ depicted in Figure 3a,b are in very good agreement, validating the fit of the superimposed $C^{4/5}$ and VC signals. The $C_1C_6Im^+$ mobility obtained from the superimposed fit of the $C^{4/5}$ signals in the first spectral region containing the ^{1}H VC signal is $(4.1 \pm 0.2)\cdot 10^{-10}$ m^2 V^{-1} s^{-1}; it matches very well the mobilities obtained from the second spectral region (2 to −0.5 ppm) analyzed via phase correction, $(4.3 \pm 0.2)\ 10^{-10}$ m^2 V^{-1} s^{-1}, and the mobility extracted by Lorentz fitting, which is $(4.2 \pm 0.2)\ 10^{-10}$ m^2 V^{-1} s^{-1}.

While $C_1C_6Im^+$ exhibits a positive slope and therefore a positive mobility, this is not the case for VC with $\mu = (-0.1 \pm 0.2)\cdot 10^{-10}$ m^2 V^{-1} s^{-1}. However, the error bars of the phase shifts of VC are large because the VC signal contributes only to a small part of the fitted region. Hence, one can conclude that in view of the given error range, VC has an electrophoretic mobility of zero.

Finally, the zero mobility of VC sheds light on the influence of solvent coordination on Li^+ migration: Previously, ^{7}Li-^{1}H heteronuclear Overhauser enhancement spectroscopy experiments had indicated a vicinity of VC with Li^+, and molecular dynamics results suggest an average contribution of 0.5 O_{VC} atoms in the first Li^+ solvation shell.[8] Thus, a coordination of VC to Li^+ is clearly evident. On the other hand, this

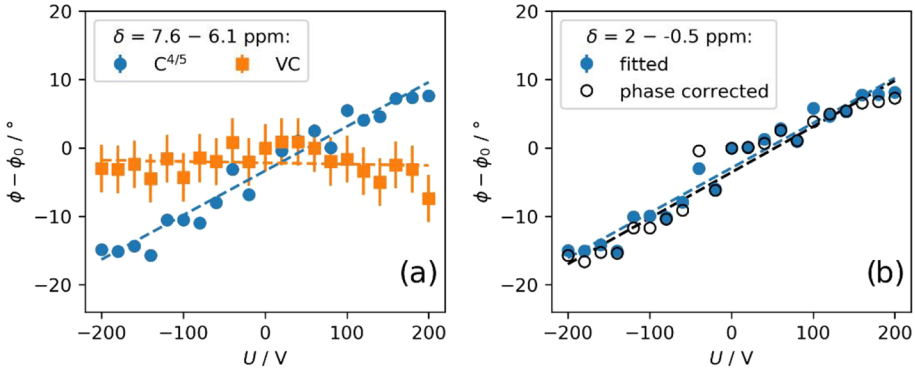

FIGURE 3 Phase shift values ϕ-ϕ_0 plotted against the applied voltages obtained from (a) fit results of the superimposed VC and $C^{4/5}$ signals observed between 7.6 and 6.1 ppm. (b) Fitted and phase-corrected phase shift values of the isolated aliphatic ^{1}H $C_1C_6Im^+$ signals observed between 2 and −0.5 ppm

coordination is not sufficiently long lived to induce a drag of VC alongside with Li^+ in the electric field.

Concerning the Li^+ transport, for Li salt in IL systems without additive, it was previously discussed whether the Li^+ transport may occur as structural transport via Li^+ ion hopping between different coordination sites (involving short-lived Li–anion coordination), or via a vehicle transport of Li-containing clusters, involving a Li–anion coordination lifetime, which is longer than the time scale of a cluster displacement.[23,26] There, long-lived coordination was found, leading to vehicle transport of Li $(Anion)_x^{1-x}$ clusters, evidenced by a negative transference number of Li.[23] In the present system containing VC, we also investigated the Li^+ migration by ^{7}Li eNMR (see Figure S2). The results show a negative Li^+ mobility, similar to the findings in salt in IL systems without added carbonate.[23] Hence, the Li^+ migration behavior is still dominated by anionic lithium–anion clusters.

Concerning the VC–Li^+ coordination, the opposite case applies: A short-lived VC–Li coordination leads to Li^+ moving between different VC coordination sites, which do not experience a drift in the electric field, while Li^+ still drifts alongside with its coordinated anions in the anion direction. The correlated motion with the anions might be, however, reduced by the VC coordination, which is possibly the cause for the improved performance of lithium-ion batteries using IL electrolytes with VC.[47]

4.3 | Tetraglyme in Li $(G4)_1(C_1C_2Im)_8TFSA_9$

The system of $Li(G4)_1(C_1C_2Im)_8(TFSA)_9$ offers another example to showcase the analysis of superimposed ^{1}H eNMR spectra via phase-sensitive spectral deconvolution. In this mixture, the tetraglyme (G4) is coordinated to the lithium ion forming a complex cation. Therefore, a nonzero electrophoretic mobility might be expected for G4, despite not carrying a charge itself. Again, two regions of the ^{1}H eNMR spectrum (see the full spectrum in Figure S3) are selected. Figure S4 shows spectra of these regions taken with the double stimulated echo sequence at different voltage values of the electric field pulse. The first spectral region (8.5–6.5 ppm) exhibits only the aromatic proton signals of $C_1C_2Im^+$, whereas the second region (4.2–2.5 ppm) exhibits a superimposed spectrum of the G4 signals and the aliphatic proton signals of $C_1C_2Im^+$.

Due to the small accessible range of phase shift values, MOSY processing yields again peaks that are very broad in the mobility domain. An analysis is shown and discussed in Figure S6.

4.4 | Lorentz fitting procedure

Phase-sensitive spectral deconvolution of the ^{1}H eNMR spectra of $Li(G4)_1(C_1C_2Im)_8(TFSA)_9$ was performed on both spectral regions. A ^{1}H eNMR spectrum of the second spectral region, including all fitted Lorentzians, is shown in Figure 4. Due to the limited spectral resolution, each signal is approximated via a single Lorentz shape in spite of the J coupling-induced multiplicity.

The first region, displayed in Figure S4a, containing only isolated $C_1C_2Im^+$ resonances, results in the phase values given by the black circles in Figure 5b, which can serve as reference values. The second region (Figure 4), exhibiting the superimposed $C_1C_2Im^+$ and G4 signals, was fitted with and without restrictions to the fit model in order to test the necessity of physically meaningful restrictions. Figure 5a gives the results of fits without any restrictions, and Figure 5b gives the results for fits with the phases set equal for peaks that correspond to the same compound. In Figure 5a, the phase shifts of the G^2 peak are not in good agreement with the G^1 and G^3 peaks. This is physically not meaningful because all three signals belong to the same molecular species. Hence, some restrictions in the fit model are necessary in order to obtain reasonable results. In Figure 5b, the phase shift of the isolated $C_1C_2Im^+$ signals, analyzed independently, is in very good agreement with that analyzed for E^1 and E^2 in the superposition region with the G4 signals. Both are resulting in a $C_1C_2Im^+$ mobility of $(14.6 \pm 0.3)\cdot10^{-10}$ $m^2\ V^{-1}\ s^{-1}$. This demonstrates that the determination of the $C_1C_2Im^+$ phase shift in the superimposed spectrum by spectral deconvolution is accurate.

The phase shift values of G4 obtained from the same fit model exhibit a shallower slope, resulting in a mobility of $(7.2 \pm 0.5)\ 10^{-10}\ m^2\ V^{-1}\ s^{-1}$ as obtained from

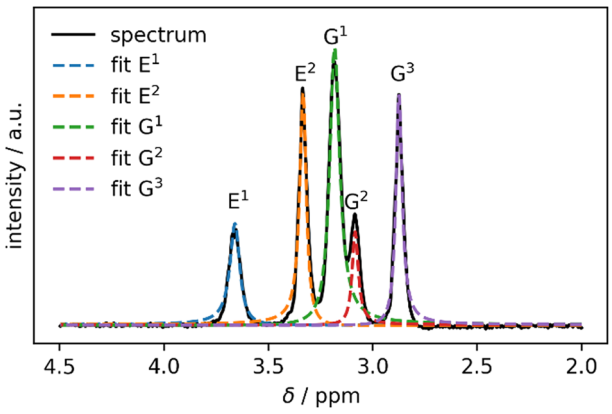

FIGURE 4 ^{1}H electrophoretic nuclear magnetic resonance spectrum of $Li(G4)_1C_1C_2Im_8TFSA_9$ showing the spectral region approximated with a set of five Lorentz distributions. E^1 and E^2 corresponding to $EMIm^+$ and G^1, G^2, and G^3 corresponding to G4

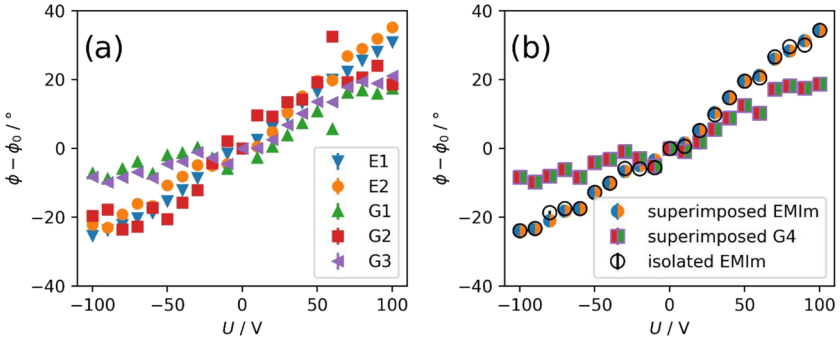

FIGURE 5 Phase shift ϕ-ϕ_0 against applied voltage obtained from superimposed ^{1}H electrophoretic nuclear magnetic resonance spectra (δ = 4.2–2.5 ppm) of $Li(G4)_1C_1C_2Im_8TFSA_9$ using (a) an unrestricted fit model and (b) a fit with identical phase values for ^{1}H resonances from the same molecule. In addition, phase shift values of the isolated $C_1C_2Im^+$ signals (δ = 8.5–6.5 ppm) are depicted in (b)

Figure 5b. Interestingly, this G4 mobility agrees well with the lithium mobility of (7.4 ± 0.7) 10^{-10} m^2 V^{-1} s^{-1} extracted from ^{7}Li eNMR experiments on the same sample (see phase shifts in Figure S5). Thus, a correlated migration of G4 with lithium in form of $(LiG4)^+$ solvate ions can be concluded in $Li(G4)_1(C_1C_2Im)_8(TFSA)_9$. Previous studies had already assumed a correlated migration of G4 with lithium as a complex solvate cation, because identical self-diffusion coefficients were observed.[36,37] Here, we show that this is not a mere coincidence of diffusivities, but indeed, the neutral G4 molecule exhibits a drift in the electric field due to its coordination to the Li^+ ion.

Furthermore, the results show that Li^+ is migrating in the expected "right" direction. The coordination with G4 apparently reduces the lithium–anion interaction and breaks the net negatively charged Li–anion clusters. G4 thus serves to form a complex solvate cation and effectively reverses the lithium migration from the wrong to the right direction.

Finally, comparing the two systems including VC and tetraglyme, respectively, major differences are obvious, which can be attributed to a very different coordination strength of the respective additive to Li^+: We recall that the additive-free Li salt in IL system exhibits a Li migration in a vehicle mechanism in form of net negatively charged Li $(Anion)_x^{1-x}$ clusters. VC as an additive in such an electrolyte does not change the direction of lithium migration, though it may weaken the Li–anion coordination somewhat. The VC itself exhibits no significant migration, but is nevertheless coordinated to Li^+; thus, these coordination bonds can be concluded to be short lived. Hence, no long-lived VC lithium clusters are formed and lithium–anion clusters are still dominating the lithium migration behavior in this mixture.

Tetraglyme, on the other hand, shows a strong coordination to Li^+, and we prove here a migration of these neutral molecules in an electric field. This is attributed to a long-lived coordination; thus, Li is dragging the tetraglyme along in the field direction. The Li–tetraglyme clusters effectively act like a cation. In addition, G4 leads to the effective breakage of negatively charged lithium–anion clusters as indicated by a positive lithium mobility.

5 | CONCLUSION

Although MOSY is a powerful tool for the analysis of superimposed eNMR spectra, its application is tied to the observable phase ranges. In eNMR experiments on ILs, this phase range is typically far below a full period. This limitation can be overcome by spectral deconvolution of eNMR spectra via a set of Lorentz profiles with absorptive and dispersive components. However, reasonable restrictions need to be introduced to the fit model in order to obtain reliable results. Using this procedure, we could for the first time analyze the transport of uncharged, coordinating solvent molecules in an electric field and distinguish between correlated or uncorrelated additive–lithium migration, respectively. Instead of indirectly deducing migration behavior from diffusion measurements, we directly observe the displacement of the investigated molecules within an electric field.

Using VC as an additive in a lithium salt IL electrolyte does not change the lithium migration mechanism significantly. Lithium is migrating, correlated with the anions in net negatively charged clusters, and is thus migrating in the wrong direction, whereas vinylene carbonate exhibits no significant migration. Hence, no long-lived VC–lithium clusters are formed and lithium–anion clusters are still dominating the lithium migration behavior in this mixture.

On the other hand, using tetraglyme as the additive in a lithium salt IL electrolyte leads to the effective breakage of negatively charged lithium–anion clusters as indicated by a positive lithium mobility. In this context, we present the first direct observation of a correlated migration of tetraglyme with lithium as a complex solvate cation, which is generally assumed in solvate ILs.

ACKNOWLEDGEMENT

We thank Professor Andrea Mele of Politecnico Milano for valuable discussions and his inspiration for initiating this project.

ORCID

Monika Schönhoff https://orcid.org/0000-0002-5299-783X

REFERENCES

[1] M. Marcinek, J. Syzdek, M. Marczewski, M. Piszcz, L. Niedzicki, M. Kalita, A. Plewa-Marczewska, A. Bitner, P. Wieczorek, T. Trzeciak, M. Kasprzyk, P. Lezak, Z. Zukowska, A. Zalewska, W. Wieczorek, *Solid State Ion.* **2015**, *276*, 107.
[2] M. Watanabe, K. Dokko, K. Ueno, M. L. Thomas, *Bull. Chem. Soc. Jpn.* **2018**, *91*, 1660.
[3] P. M. Bayley, G. H. Lane, N. M. Rocher, B. R. Clare, A. S. Best, D. R. MacFarlane, M. Forsyth, *Phys. Chem. Chem. Phys.* **2009**, *11*, 7202.
[4] P. M. Bayley, G. H. Lane, L. J. Lyons, D. R. MacFarlane, M. Forsyth, *J. Phys. Chem. C* **2010**, *114*, 20569.
[5] M. L. P. Le, L. Cointeaux, P. Strobel, J.-C. Leprêtre, P. Judeinstein, F. Alloin, *J. Phys. Chem. C* **2012**, *116*, 7712.
[6] A. Deshpande, L. Kariyawasam, P. Dutta, S. Banerjee, *J. Phys. Chem. C* **2013**, *117*, 25343.
[7] A. Eilmes, P. Kubisiak, *J. Phys. Chem. B* **2015**, *119*, 11708.
[8] E. Bolimowska, F. Castiglione, J. Devemy, H. Rouault, A. Mele, A. A. H. Pádua, C. C. Santini, *J. Phys. Chem. B* **2018**, *122*, 8560.
[9] Z. Li, O. Borodin, G. D. Smith, D. Bedrov, *J. Phys. Chem. B* **2015**, *119*, 3085.
[10] S. Jeremias, M. Kunze, S. Passerini, M. Schönhoff, *J. Phys. Chem. B* **2013**, *117*, 10596.
[11] M. Brinkkötter, E. I. Lozinskaya, D. O. Ponkratov, P. S. Vlasov, M. P. Rosenwinkel, I. A. Malyshkina, Y. Vygodskii, A. S. Shaplov, M. Schönhoff, *Electrochim. Acta* **2017**, *237*, 237.
[12] K. Yoshida, M. Tsuchiya, N. Tachikawa, K. Dokko, M. Watanabe, *J. Electrochem. Soc.* **2012**, *159*, A1005.
[13] M. Gouverneur, J. Kopp, L. van Wüllen, M. Schönhoff, *Phys. Chem. Chem. Phys.* **2015**, *17*, 30680.
[14] M. Kunze, Y. Karatas, H.-D. Wiemhöfer, M. Schönhoff, *Macromolecules* **2012**, *45*, 8328.
[15] J. Popovic, C. Pfaffenhuber, J. P. Melchior, J. Maier, *Electrochem. Commun.* **2015**, *60*, 195.
[16] K. Ueno, H. Tokuda, M. Watanabe, *Phys. Chem. Chem. Phys.* **2010**, *12*, 1649.
[17] J. Maier, *Electrochim. Acta* **2014**, *129*, 21.
[18] N. A. Stolwijk, J. Kösters, M. Wiencierz, M. Schönhoff, *Electrochim. Acta* **2013**, *102*, 451.
[19] Z. Zhang, L. A. Madsen, *J. Chem. Phys.* **2014**, *140*, 084204.
[20] M. Holz, *Chem. Soc. Rev.* **1994**, *23*, 165.
[21] P. C. Griffiths, *Annual Reports on NMR Spectroscopy* **2009**, *65*, 139.
[22] U. Scheler, *eMagRes* **2012**, *1*. https://doi.org/10.1002/9780470034590.emrstm0154.pub2
[23] M. Gouverneur, F. Schmidt, M. Schönhoff, *Phys. Chem. Chem. Phys.* **2018**, *20*, 7470.
[24] J. C. Lassegues, J. Grondin, D. Talaga, *Phys. Chem. Chem. Phys.* **2006**, *8*, 5629.
[25] N. Molinari, J. P. Mailoa, B. Kozinsky, *J. Phys. Chem. Lett.* **2019**, *10*, 2321.
[26] M. Brinkkötter, G. A. Giffin, A. Moretti, S. Jeong, S. Passerini, M. Schönhoff, *Chem. Commun.* **2018**, *54*, 4278.
[27] K. F. Morris, C. S. Johnson, *J. Am. Chem. Soc.* **1992**, *114*, 776.
[28] Y. Fang, P. V. Yushmanov, I. Furo, *Magn. Reson. Chem.* **2017**, *55*, 584.
[29] Q. H. He, C. S. Johnson, *J. Magn. Reson.* **1989**, *81*, 435.
[30] D. J. States, R. A. Haberkorn, D. J. Ruben, *J. Magn. Reson.* **1982**, *48*, 286.
[31] U. Böhme, A. Klenge, B. Hanel, U. Scheler, *Polymers* **2011**, *3*, 812.
[32] U. Böhme, U. Scheler, *Adv. Colloid. Interfac.* **2010**, *158*, 63.
[33] U. Böhme, U. Scheler, *Macromol. Symp.* **2004**, *211*, 87.
[34] U. Scheler, U. Böhme, *Abstr. Pap. A. Chem. S.* **2003**, *225*, U631.
[35] S. Wong, U. Scheler, *Colloid Surface A* **2001**, *195*, 253.
[36] K. Ueno, K. Yoshida, M. Tsuchiya, N. Tachikawa, K. Dokko, M. Watanabe, *J. Phys. Chem. B* **2012**, *116*, 11323.
[37] K. Yoshida, M. Nakamura, Y. Kazue, N. Tachikawa, S. Tsuzuki, S. Seki, K. Dokko, M. Watanabe, *J. Am. Chem. Soc.* **2011**, *133*, 13121.
[38] A. Jerschow, N. Müller, *J. Magn. Reson.* **1997**, *125*, 372.
[39] T. Cremer, C. Kolbeck, K. R. J. Lovelock, N. Paape, R. Wölfel, P. S. Schulz, P. Wasserscheid, H. Weber, J. Thar, B. Kirchner, F. Maier, H.-P. Steinrück, *Chem. A Eur. J.* **2010**, *16*, 9018.
[40] J. J. Helmus, C. P. Jaroniec, *J. Biomol. NMR* **2013**, *55*, 355.
[41] J. Keeler, *Understanding NMR Spectroscopy*, Wiley, Chichester **2011**.
[42] R. R. Ernst, *J. Magn. Reson.* **1969**, *1*, 7.
[43] J. Van Vaals, P. Van Gerwen, *J. Magn. Reson.* **1990**, *86*, 127.
[44] D. E. Brown, T. W. Campbell, R. N. Moore, *J. Magn. Reson.* **1989**, *85*, 15.
[45] A. Heuer, *J. Magn. Reson.* **1991**, *91*, 241.
[46] L. Chen, Z. Q. Weng, L. Y. Goh, M. Garland, *J. Magn. Reson.* **2002**, *158*, 164.
[47] H. Srour, H. Rouault, C. Santini, *J. Electrochem. Soc.* **2013**, *160*, A66.

SUPPORTING INFORMATION

Additional supporting information may be found online in the Supporting Information section at the end of this article.

How to cite this article: Schmidt F, Pugliese A, Santini CC, Castiglione F, Schönhoff M. Spectral deconvolution in electrophoretic NMR to investigate the migration of neutral molecules in electrolytes. *Magn Reson Chem*. 2020;58:271–279. https://doi.org/10.1002/mrc.4978